Power Density Optimization of Resonant Tanks Using Standard Capacitors

Phyo Aung Kyaw, Aaron L.F. Stein, Charles R. Sullivan
Thayer School of Engineering at Dartmouth
Hanover, NH 03755, USA
{phyo.a.kyaw.th, aaron.l.stein, charles.r.sullivan}@dartmouth.edu

***Abstract*—High-frequency power conversion is useful for miniaturization of power electronics, but requires low loss passive components to achieve high power densities without thermal issues. This paper investigates the lowest achievable ESR of a resonant tank using an air-core inductor with a single-layer foil winding and commercially available capacitors. A loss model is presented and online catalogs of multilayer ceramic capacitors are searched for components that can provide a low ESR when combined with an optimally designed inductor for various resonance frequencies. The resulting resonator has a measured sub-mΩ ESR and high efficiency with 250 V dc rating in a 1 cm^3 volume. The resonant tank, when used in a resonant switched-capacitor converter, can theoretically handle up to 12 kW assuming a tolerable loss of 2 W, and the power converter itself will be limited by the power density of switches and interconnects rather than by passive components.**

I. Introduction

Recent advances in wide-bandgap semiconductors such as GaN and SiC that allows for efficient high-frequency power conversion mean that passive components are increasingly becoming the main bottleneck in the miniaturization of power electronics through high switching frequency [1], [2]. Improvements in both capacitor and inductor technologies are required to eliminate this bottleneck. Capacitors have a trade-off among dielectric constant, breakdown electric field and dissipation factors of dielectric materials; recent research activities focus on improving all three factors simultaneously by investigating alkali-free glass dielectric [3] and developing nanocomposites of high-breakdown-field polymers and high-dielectric-constant ceramics [4], [5]. For magnetics, new and improved magnetic materials are required to reduce high-frequency core loss, and a multi-layer foil winding with equal current sharing can provide significant improvement in skin and proximity effect losses [6]–[8].

Assuming optimistically that these advances in dielectric and magnetic materials become practical and that multi-layer foil windings can be implemented without requiring additional space or incurring extra losses, the resulting combination is a low-loss high-power-density resonator with significant improvement over today's passive components [9]. However, the analysis in [9] is an optimistic assessment; the implementation of such a resonator requires significant research and development effort in improving dielectric and magnetic materials and inductor windings. A practical LC resonator using currently available materials can be analyzed by incorporating skin effect and losses of commercially available capacitors into the analysis of [9]. Such an analysis can illuminate currently achievable performance of LC resonators and the necessary improvement in capacitor and inductor technologies to go beyond that limit.

In this paper, we present an LC resonant tank with low loss and high power density using off-the-shelf capacitors and a single-layer foil winding. We present the design objectives for the resonant tank in Section II. A loss model is derived in Section III for an LC resonator assuming a skin-depth limit and performance of commercially available capacitors. Section IV describes the design process that uses this loss model for choosing reference capacitors which can provide very low loss, and optimizing the inductor design with respect to total loss for resonant tanks using these reference capacitors. The loss model and the optimal inductor designs are then verified by an experiment in Section V; the test resonator has a sub-mΩ ESR and a very high efficiency in a $1\ \mathrm{cm}^3$ volume. Power conversion applications for this resonator and corresponding limitations are discussed in Section VI. The resonator is useful in resonant switched-capacitor converters and can theoretically handle up to $12\ \mathrm{kW}$ assuming a tolerable loss of $2\ \mathrm{W}$; the density of such a power converter will be limited by switches and interconnects, and not by the resonant tank.

II. Design Objective

The achievable power density of an LC resonant tank depends on the current capability, limited by the thermal effect of loss, and the allowed voltage, limited by dielectric breakdown in the capacitors. In power converter topologies such as resonant switched-capacitor (ReSC) circuits [10], [11], the required voltage capability depends on the required input and output voltages. Thus, the thermal effect of loss and the loss in the resonant tank itself need to be minimized to achieve a high power density.

Because losses can be lowered by increasing the available volume, the total volume of the resonant tank is limited to $\mathcal{V}$ to standardize the analysis. A fraction r_v of this volume is reserved for the inductor, whose dimensions need to be optimized to achieve a low loss for the desired inductance and the operating frequency. Only air-core inductors are considered because of high losses in magnetic materials for operation at MHz frequencies. The winding is limited to a single-layer conductor with a skin-depth thickness to minimize proximity

effect losses. The remaining volume $(1-r_v)\mathcal{V}$ is filled by the capacitor. The choice of capacitor is important since it impacts not only the capacitor losses but also the required inductance, hence the inductor losses. A low dissipation factor is necessary to minimize the capacitor losses and a high energy density is needed to reserve as big a volume possible for the inductor which is usually more lossy than capacitors.

State-of-the-art dielectric materials such as alkali-free glass dielectric [3] have a high energy density of $38\ \mathrm{J/cm^3}$ without derating. However, we limit the analysis to commercially available C0G and X7R capacitors to examine the possible performance using currently available technology and materials. The capacitor energy density can be repesented by choosing a particular capacitor from an online catalog as a reference, with capacitance C_{ref}, voltage rating V_{ref}, volume $\mathcal{V}_{ref}$, energy density u_{ref} and dissipation factor D_{ref}. The required capacitance for the resonant tank can be achieved by proportionally scaling the reference capacitor dimensions. In the simplest model, we assume that the capacitor energy density and dissipation factor remain unchanged for different capacitance values and physical sizes. The reference capacitor choice will affect the energy density of the capacitor required for the resonant tank, hence the achievable loss and power density. For the reference capacitor, the resonator design can be optimized for maximum power density by minimizing loss.

III. Loss Model

Using reference capacitors with an energy density u_{ref}, the resulting capacitance C and the effective series resistance (ESR) R_C of the capacitor inside a volume $(1-r_v)\mathcal{V}$ is

$$C = \frac{2u_{ref}(1-r_v)\mathcal{V}}{V^2} \propto \frac{u_{ref}}{V^2}, \tag{1}$$

$$R_C = \frac{D_{ref}}{2\pi f C} \propto \frac{1}{C} \propto \frac{V^2}{u_{ref}}, \tag{2}$$

where V is the dc voltage rating of the resonator and f the desired resonance frequency. The capacitor ESR depends on the total capacitance, and is proportional to the desired dc voltage rating squared V^2 and inversely proportional to the reference capacitor energy density u_{ref}.

For the resonance frequency f, the inductance needs to be

$$L = \frac{1}{4\pi^2 f^2 C} \propto \frac{V^2}{u_{ref}}. \tag{3}$$

The inductor design can be divided into two regimes. For a low resonance frequency where a high inductance is required, the inductor is a multi-turn large-area ring or square loop, as shown in Fig. 1 (a). As the frequency increases and the required inductance decreases, the number of turns decreases to unity and the inductor becomes narrower and longer as shown in Fig. 1 (b) [9]. The inductor loss model depends on whether it is multi-turn or single-turn.

A. Low Frequency Inductor Model

For the low-frequency high-inductance case, the inductor design, specifically the number of turns N, the inductor

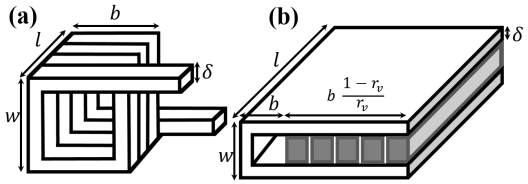

Fig. 1. Resonator sketches. (a) Inductor design for low frequency and high inductance. (b) Parallel resonator design for high frequency and low inductance; the inductor wraps around the capacitors.

volume as a fraction of the total volume r_v, and the geometric dimensions l, b and w, need to be chosen such that

$$L = \frac{N^2\mu_0 wb}{l} = \frac{N^2\mu_0 w^2 b^2}{r_v\mathcal{V}}, \tag{4}$$

where L is given by (3), μ_0 is the vacuum permeability and the second equality is derived from the volume constraint $lbw = r_v\mathcal{V}$. If the required inductance is sufficiently large, the capacitor self-inductance, usually on the order of nH, can be ignored. The inductor ESR R_L, assuming that the thickness of the conductor is equal to the skin-depth δ ($\ll w,\ b$), is

$$\begin{aligned} R_L &= \frac{\rho}{l\delta}\left(N^2(2w+2b) - Nw + 2b\frac{1-r_v}{3r_v}\right) \\ &= \frac{\rho wb}{r_v\mathcal{V}\delta}\left(N^2(2w+2b) - Nw + 2b\frac{1-r_v}{3r_v}\right) \qquad (5) \\ &\propto L \propto \frac{V^2}{u_{ref}}, \qquad (6) \end{aligned}$$

where ρ is copper resistivity. The second term corrects for the lack of a vertical segment in one turn and the last term adds the resistance of the conductor with which the capacitors are connected to the inductor.

For a sufficiently low frequency, the required inductance is large, which usually requires $N \gg 1$. In such cases, it is shown in [9] that the inductance is mostly impacted by changing the number of turns N and not the geometric dimensions, resulting in $L \propto N^2$. Moreover, for $N \gg 1$, the N^2 term in (5) is dominant and the optimal inductor has a square cross section ($w = b$) since w and b are qualitatively equal, resulting in $R_L \propto N^2$. Because N is the dominant factor at low frequency, and both R_L and L are proportional to N^2, we can conclude that

$$R_L \propto L \propto \frac{V^2}{u_{ref}}, \tag{7}$$

B. High Frequency Inductor Model

For the high-frequency low-inductance regime, the inductor is a single-turn small-area long solenoid shown in Fig. 1 (b) [9]. Because the inductor loop is only a single-turn, the capacitor volume also contributes significantly to the total inductance. Thus, we need to choose the inductor design (r_v, l, b, w) such that

$$L = \frac{\mu_0 w}{l}\left(b + b\frac{1-r_v}{3r_v}\right) = \frac{\mu_0 w^2 b^2}{r_v\mathcal{V}}\frac{1+2r_v}{3r_v}, \tag{8}$$

where the factor $b(1-r_v)/(3r_v)$ gives the first-order approximation for the effective breadth of the capacitors that

contribute to the total inductance. The factor of 3 arises from the assumption that the current is equally distributed among all the electrode plates of the capacitor, resulting in a magnetic field that increases linearly and a magnetic energy density that increases quadratically along b, which when integrated gives a factor of 3 in the denominator. Using (5), the inductor ESR R_L for $N = 1$ can be rewritten as

$$R_L = \frac{\rho w b}{r_v \mathcal{V} \delta} \left(w + 2b \frac{1 + 2r_v}{3r_v} \right). \tag{9}$$

Because the capacitor can have self-inductance on the same order of magnitude as the inductor, a larger fraction of the available volume can be reserved for the capacitor than in the low-frequency case. This increases the achievable capacitance which in turn decreases the required inductance. Thus, it can be shown that the optimum fraction of the volume that should be reserved for the inductor is zero (i.e. $r_{v,opt} = 0$); Appendix A shows the detailed derivation. Thus, (8) and (9) can be rewritten in term of the resonator total breadth b_{tot}:

$$L = \frac{\mu_0 w^2 b_{tot}^2}{3\mathcal{V}}, \tag{10}$$

$$R_L = \frac{\rho w b_{tot}}{\mathcal{V} \delta} \left(w + \frac{2b_{tot}}{3} \right). \tag{11}$$

The inductor ESR can be minimized by substituting wb_{tot} from (10) into (11) and differentiating R_L with respect to b_{tot}. This gives

$$R_{L,opt} \propto L^{3/4} \propto \left(\frac{V^2}{u_{ref}} \right)^{3/4}, \tag{12}$$

and Appendix B shows the detailed derivation.

IV. Design Process

According to the loss model in Section III, we need to choose a high dc voltage rating and capacitors with a high energy density to design a resonant tank with a high power density. Normalizing the total ESR with the dc voltage rating shows that the higher the energy density, the lower the total ESR. However, capacitors with a high energy density also tend to have a high dissipation factor and are less stable, especially at high frequencies. Thus, it is important to consider the trade-off between high energy density and low dissipation factor. In this paper, we examine the achievable ESR for resonators using two capacitor types, namely C0G and X7R capacitors.

A. Choosing high-energy density capacitors

Fig. 2 shows the maximum nominal energy density u_{ref} for various dc voltage rating V_{ref} of commercially available surface mount C0G and X7R capacitors on Digi-Key catalog [12]. Only the nominal energy density is considered here since a capacitor with the maximum energy density is to be selected for each capacitor type. The nominal energy density is calculated using the capacitance value at the bias voltage, and is representative of the capacitor's performance if the voltage ripple is small compared to the bias voltage. The actual energy density would be of interest for accurate modeling if the capacitors are fully charged and discharged during each cycle, and can be calculated by integrating the QV curve of the capacitors as done in [13].

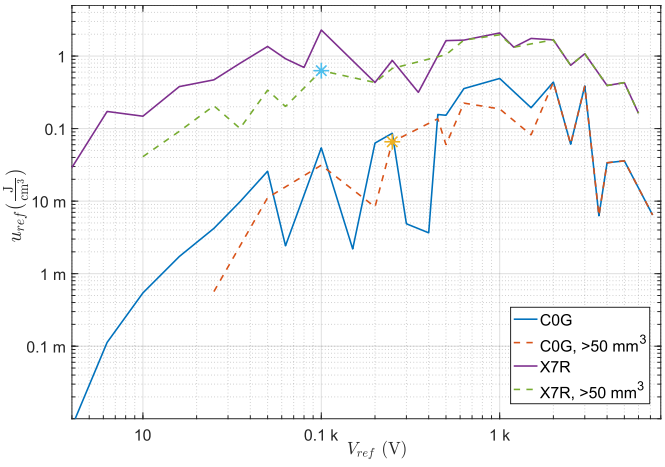

Fig. 2. Maximum nominal energy density of C0G and X7R capacitors as a function of the rated dc voltage. The dashed lines represent the corresponding plots for capacitors larger than 50 mm^3. The asterisks represent the reference capacitors used in this paper.

Because many capacitors may need to be connected in parallel to achieve a high capacitance, only C0G capacitors larger than 100 pF and X7R capacitors larger than 1 nF are included in Fig. 2. C0G capacitors have about one to two orders of magnitude lower energy density than X7R capacitors with the same voltage rating. C0G capacitors can have an energy density as high as 0.5 $\mathrm{J/cm}^3$, with 1 kV rating, and X7R capacitors 2.2 $\mathrm{J/cm}^3$, with 100 V rating. The choice of voltage rating V_{ref} of the reference capacitor is also important since high-energy-density capacitors are not readily available at some voltage ratings. For example, the maximum energy density for 150 V rated C0G capacitors in the Digi-Key catalog is only around 2 $\mathrm{mJ/cm}^3$ whereas those for 100 V and 200 V ratings are about 30 times higher, at around 60 $\mathrm{mJ/cm}^3$.

For ease of building a prototype resonator of about 1 cm^3, the capacitor search was repeated with a minimum volume limit of 50 mm^3 so that no more than 20 reference capacitors need to be connected in parallel within the available volume. The highest energy density of commercially available capacitors with this volume constraint are also included in Fig. 2. Limiting the volume to be at least 50 mm^3 reduces the energy density of readily available capacitors by as much as a factor of 5 for voltage ratings below 500 V. If we also limit the dc voltage rating to be lower than the 3-400 V range to address a wide range of applications, the capacitors with largest energy density correspond to a 250 V rating for both C0G and X7R. However, we chose a 100 V rating as the reference for X7R capacitors since they have 93% the energy density of 250 V X7R capacitors. Table I shows the specifics for the 250 V C0G and 100 V X7R capacitors chosen as the reference.

B. Dissipation factors

The dissipation factors for these reference capacitors were extracted from TDK SEAT 2013 [14] and AVX Spicap 3.0 [15] software. The ESR data from the software was divided by

TABLE I
CAPACITOR SPECIFICS

Type	V_{ref} (V)	Manufacturer	Part Number	C_{ref}(µF)	u_{ref} (mJ/cm^3)	Dimensions (mm × mm × mm)
C0G	250	TDK	CGA9N4C0G2E154J230KN	0.15	65.8	5.7 × 5 × 2.5
X7R	100	AVX	22201C106MAT2A	10	628.8	5.7 × 5 × 2.79

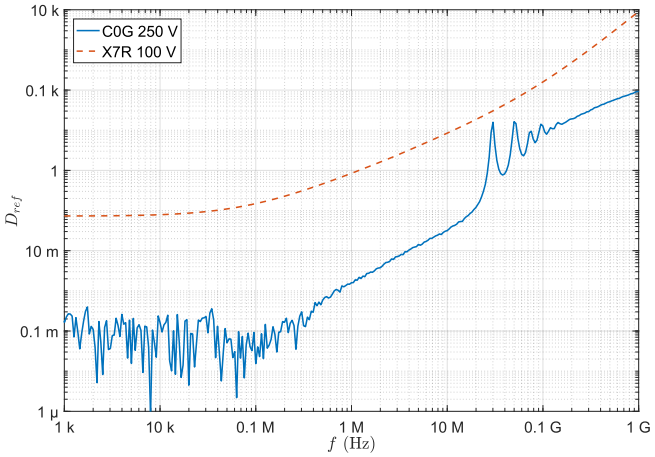

Fig. 3. Frequency characteristic of the dissipation factor of C0G and X7R capacitors in Table I.

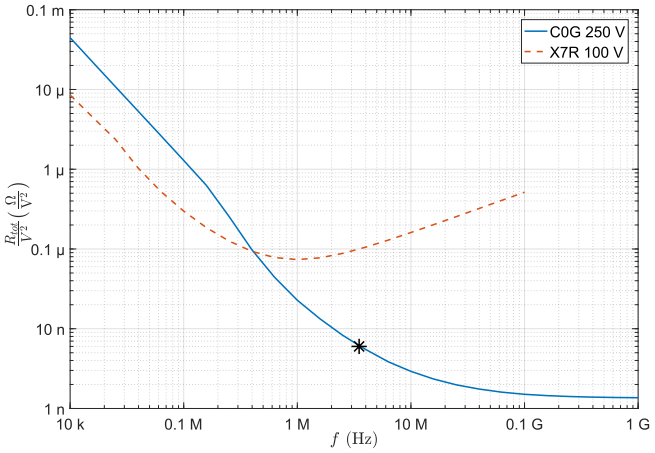

Fig. 4. Minimum achievable ESR as a function of resonance frequency for the C0G and X7R capacitors in Table I.

the reference capacitor impedance $2\pi f C_{ref}$ to obtain the dissipation factor D_{ref} shown in Fig. 3. Even though the X7R reference capacitor has about an order of magnitude higher nominal energy density than the C0G reference capacitor, the dissipation factor is about two orders of magnitude higher at all frequencies. Thus, the advantages of the X7R capacitor's higher energy density will disappear if the higher dissipation factor causes the capacitor ESR to dominate the inductor ESR.

The dissipation factors D_{ref} as shown in Fig. 3 are higher than unity at frequencies $\gtrsim 25$ MHz for the C0G capacitors and $\gtrsim 1$ MHz for the X7R capacitors. These frequencies correspond to the self-resonant frequencies above which the capacitor self-inductance dominates the capacitive impedance. Because D_{ref} is defined in this paper as the ratio between the capacitor ESR and the capacitive impedance, the low capacitive impedance above the self-resonant frequency translates to a dissipation factor greater than 1. However, these dissipation factors greater than 1 are still valid in terms of loss calculation so long as the capacitive impedance, rather than the capacitor's self-inductive impedance, is used to calculate the ESR.

C. Resonator Design Optimization

Particle swarm optimization is performed on the total ESR of the inductor and the capacitors for a fixed 1 cm^3 volume at various frequencies. In order to correctly represent the transition between the low-frequency and high-frequency regimes, the self-inductance of the capacitor as well as the inductance of the inductor are included in calculating L. Similarly, R_L in (5) is used in the optimization since it correctly accounts for the ESR of the inductor and the resistance of the conductor with which the capacitors are connected to the inductor. The actual energy density of X7R capacitors, obtainable from TDK SEAT 2013 [14] and AVX Spicap 3.0 [15] design tools, is used in the optimization.

This optimization gives the minimum achievable ESR for 1 cm^3 LC resonators as shown in Fig. 4, and the corresponding inductor design to obtain that ESR. As predicted by the loss model, most of the design differences along each R vs. f curve at the lower frequency end are due to changes in the number of turns N. As the frequency gets higher, the capacitor self-inductance starts to become significant. And as derived in Appendix A, the optimum resonator design does not require a separate inductor (i.e. $r_{v,opt} \approx 0$) to achieve the desired resonance frequency.

At the lower frequency end, the inductor ESR dominates the capacitor ESR because of the large number of turns required. Thus, the higher dissipation factor of the X7R capacitor compared to that of the C0G capacitor has an insignificant impact on the overall ESR since D_{ref} only changes the capacitor ESR. However, the energy density impacts the ESR of both the capacitor and the inductor; thus, the resonator with the X7R reference capacitor has a lower ESR than that with the C0G reference capacitor at the lower frequency end.

As D_{ref} gets larger at higher frequencies, the capacitor ESR becomes more significant and the resonator with the C0G capacitor has a lower overall ESR than that with the X7R capacitor because of the lower dissipation factor. The crossover point between the two regimes occur ~ 400 kHz. Thus, for power conversion at MHz frequencies, low-energy-density capacitors with low dissipation factors can outperform high-energy-density capacitors with high dissipation factors.

V. EXPERIMENTAL VERIFICATION

We verified the loss model and the optimization results by building a prototype resonator along one of the curves in Fig. 4. We chose the design represented by the asterisk

Fig. 5. The parallel resonator.

TABLE II
PREDICTED AND MEASURED RESULTS

	Predicted	Measured	
		No Core	With Core
L (nH)	1.2	1.48	1.89
C (µF)	2.4	2.35	2.35
f (MHz)	2.97	2.70	2.40
R_L (mΩ)	0.28	0.56	0.45
R_C (mΩ)	0.16		

in Fig. 4. The chosen design uses C0G capacitors and gives a resonance frequency of 3.5 MHz with 0.38 mΩ ESR (6 nΩ/V^2 at 250 V). This design point was chosen because it has a low ESR (sub-mΩ) in the MHz frequency range, and higher frequency operation only reduces the ESR by an additional 0.3 mΩ because of the knee in the R vs. f curve (Fig. 4). The lower ESR at higher frequencies will also be more difficult to measure.

The design requires connecting 14 reference C0G capacitors (Table I) in a 4×3.5 grid which is not feasible without custom fabricated capacitors. Thus, we chose instead to connect 16 capacitors in a 4×4 grid. This increases the total volume to 1.14 cm^3 which means the C0G curve in Fig. 4 is slightly shifted down. This resonator with 16 capacitors is shown in Fig. 5, and has 5.7 mm × 1 cm × 2 cm dimensions. The resonator is predicted to have $L = 1.2$ nH, $C = 2.4$ µF, $f = 2.97$ MHz, $R_L = 0.28$ mΩ and $R_C = 0.16$ mΩ; the predicted values are also included in Table II.

We built a parallel resonator for experimental verification considering ease of measuring the parallel impedance at resonance. A series resonator with a similar ESR can be obtained by removing the copper foil at the top.

A frequency sweep of the resonator impedance is obtained using an Agilent 4294A impedance analyzer, and the measured impedance is shown in Fig. 6. The fundamental parallel resonance occurs at 2.7 MHz, resulting in $L = 1.48$ nH for a measured $C = 2.35$ µF. Using these L and C values, the peak impedance of $R_p = 1.13$ Ω can be translated into the total ESR as $R_{tot} = L/(CR_p) = 0.56$ mΩ (Table II).

The inductance calculated from the measured resonance frequency and capacitance is about 0.28 nH ($\sim 23\%$) larger than the inductance predicted by the loss model. This difference arises because the thickness of the solder connecting the capacitors is not accounted for in the loss model, which uses the base capacitor dimensions to calculate the inductance. This

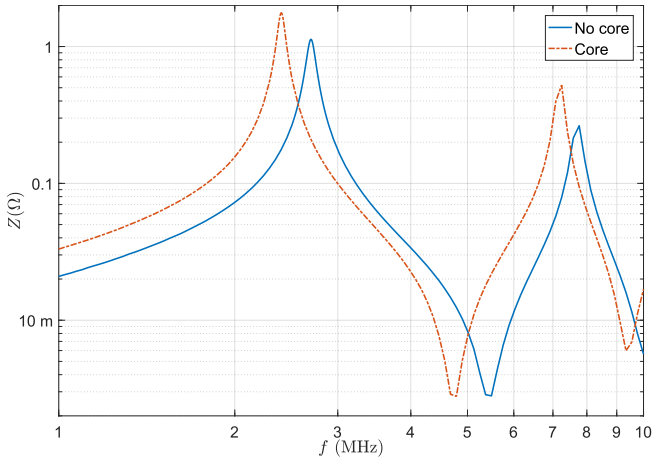

Fig. 6. Frequency characteristics of the impedance of the parallel resonator in Fig. 5, measured without and with magnetic cores of Fair-Rite 67 material.

difference in inductance also causes a discrepancy between the predicted and measured resonance frequencies. There is also a 0.12 mΩ (27%) difference between the measured ESR and the loss model prediction. This difference may be attributed to the current crowding at the edges of the conductors due to fringe magnetic field lines whereas the loss model assumes that magnetic field lines are parallel to the conductors.

A. *Current crowding due to non-parallel field lines*

The effect of current crowding on the total ESR of the resonator can be experimentally investigated by placing blocks of low-loss magnetic materials at the two ends of the resonator. The magnetic cores straighten out the magnetic field lines and make them more parallel to the capacitor electrode plates. We used two blocks of Fair-Rite 67 material, which has a low loss at MHz frequencies. The frequency sweep of the resonator with cores at the end is also included in Fig. 6. The resonator has a peak parallel impedance of 1.76 Ω at 2.40 MHz, which gives $L = 1.89$ nH and $R_{tot} = 0.45$ mΩ (Table II). This value of measured R_{tot} with the magnetic cores closely matches the 0.44 mΩ total ESR predicted by the loss model.

The measured ESR with the magnetic core verifies that the loss model is accurate if the magnetic field lines are parallel to the conductors in the resonator such that there is no current crowding at the edges of the conductor. If the field lines are not parallel to the conductors, the loss model will underestimate the total resonator ESR. Finite element analysis (FEA) can be performed to check that losses introduced by current crowding are tolerable. However, accurate FEA requires information on thickness of the capacitor electrode plates and dielectric, number of dielectric layers and properties of the dielectric material used in the capacitor. In this paper, we simply used the manufacturer-provided capacitor ESR data to calculate R_C since the data usually accounts for both dielectric loss and capacitor electrode plate losses at MHz frequencies. However, finite element simulation is still needed since the interactions between the capacitors may affect the magnetic field configuration. Thus, the loss model in this paper is only for the best case scenarios in which the field lines and the

conductor plates are parallel to each other; however, it may still be used as an approximate model for cases in which the field lines and the conductor plates are not parallel.

VI. Application in Power Converters

Performance of power converters is usually limited by passive components, especially magnetics, which usually have relatively large sizes and losses. In this paper, we presented a loss model of an LC resonant tank and optimized its design to achieve a low-loss high-power-density resonator. The prototype resonator is an integrated LC tank with a sub-$\mathrm{m}\Omega$ ESR, using C0G capacitors with a 250 V rating, and the self-inductance of the capacitors rather than a separate lumped inductor. Because of the very low ESR in a $1\ \mathrm{cm}^3$ volume, a resonant power converter using this resonator can, in some cases, be limited by switches and interconnects rather than the resonator itself. Here, we describes the advantages and limitations of using this resonator in two different power converter topologies, namely series resonant converters and resonant switched-capacitor (ReSC) converters.

A. Series Resonant Converters

Series resonant converters require the loaded quality factor of the resonator to be sufficiently high in order to provide approximately sinusoidal resonator output waveforms. This requires the characteristic impedance of the resonant tank to be at least a few times higher than the desired load impedance. The presented resonant tank without the cores has a characteristic impedance of $\sqrt{L/C} = 25.1\ \mathrm{m}\Omega$ and with magnetic cores, $\sqrt{L/C} = 28.4\ \mathrm{m}\Omega$. Thus, if we assume that the characteristic impedance needs to be at least 5 times higher than the load impedance ($Q_{loaded} > 5$), the maximum load this resonator can support is around 5 $\mathrm{m}\Omega$ without the cores or 5.7 $\mathrm{m}\Omega$ with the cores. This is in general too low a load impedance for useful power conversion, so the particular implementation of resonant tank presented in this paper is not optimized for use in series resonant converters.

However, a similar optimization could be performed with a constraint on loaded quality factor to develop resonant structures for series resonant converters. The optimization can use the same loss model presented in (4), (5), (8) and (9), but the required inductance, and the corresponding inductor ESR, will be bounded from below by the required loaded Q. The dc voltage withstand capability requirement for the capacitor would also be reduced.

B. Resonant Switched-Capacitor Converters

Unlike series resonant converters, resonant switched-capacitor converters do not have a minimum requirement on the loaded quality factor of the resonant tank. The performance of ReSC converters is usually expressed by the effective output resistance R_{eff}, which is usually proportional to the resonator ESR [11], [16], [17]. For a 2:1 ReSC converter, the constant of proportionality is $\pi^2/8$, resulting in $R_{eff} = \pi^2 R_{tot}/8$.

Assuming a 2:1 ReSC converter, the 0.45 $\mathrm{m}\Omega$ measured ESR translates into a 0.56 $\mathrm{m}\Omega$ effective output impedance attributable to the resonator. With the capacitors rated at 250 V, the input and output voltages can, with some derating, be 400 V and 200 V respectively. The only other limitation for the resonator performance is the thermal effect of loss. If we assume that a 2 W loss is tolerable considering the volume and the surface area, the resonant tank can handle up to about 66.7 A rms current or 60 A output dc current. Thus, this resonator can, in theory, handle up to around 12 kW output power without dielectric breakdown or thermal issues.

Although the presented resonant tank can handle up to 66.7 A rms current due to the sub-$\mathrm{m}\Omega$ ESR, the same current through switches and interconnects in a power converter using this resonator may cause thermal issues depending on the on-resistance of the switches and the conduction resistance of the interconnects. Although wide band-gap semiconductors offer fast switching and low parasitic capacitance, these would also pose challenges with present technology at 2.4 MHz and 200 V. Considering the 12 kW capability of the resonant tank in a $1\ \mathrm{cm}^3$ volume, it can be concluded that passive components are not going to be the limiting factor in a ReSC converter using this resonant tank.

VII. Conclusion

We derived a general loss model for an LC resonant tank and used it to design a low-loss resonator using commercially available C0G and X7R capacitors. With a single-layer foil winding for the inductor, the resonator design above 1 MHz is limited by the capacitor ESR. Thus, the capacitor choice for a low ESR requires not only a high energy density but also a sufficiently low dissipation factor. The C0G capacitor of choice outperforms the X7R capacitor above 400 kHz. The prototype resonator has an experimental ESR of $0.45\ \mathrm{m}\Omega$ at around $2.4\ \mathrm{MHz}$, and the measured ESR closely matches the loss model prediction. This resonator, used in a 2:1 resonant switched-capacitor circuit, can provide up to 60 A output dc current and 12 kW output power with only 0.02% loss in the resonant tank itself.

This resonator verifies that a low-loss high-power-density resonant tank for MHz frequencies can be built using a single-layer foil conductor and commercially available capacitors. The exact design of the resonator depends on the specific power conversion applications. The presented resonator will only have limited applications in power converters such as series resonant converters which require some minimum loaded quality factor. However, it is applicable to power converters such as resonant switched-capacitor circuits, which do not pose such a limit on the minimum loaded quality factor.

Appendix A
Optimal r_v for high-frequency inductor model

In this section, we derives the optimal fraction r_v of available LC tank volume that should be reserved for the inductor. The derivation assumes single-turn low-inductance inductors required for high-frequency operation. The resulting optimal r_v is used in Section III-B to derive the relation between L and R_L of the inductor in the resonant tank.

It follows from (1) and (3) that

$$L = \frac{V^2}{8\pi^2 f^2 u_{ref}(1-r_v)\mathcal{V}} = \frac{k_1}{1-r_v}, \text{ where} \quad (13)$$

$$k_1 = \frac{V^2}{8\pi^2 f^2 u_{ref}\mathcal{V}}, \quad (14)$$

where V is the resonant tank voltage rating, u_{ref} the energy density of the reference capacitor, and $\mathcal{V}$ the available volume. Substituting (13) into (8) gives

$$\begin{aligned} wb &= \sqrt{\frac{3k_1\mathcal{V}}{\mu_0}}\ \frac{r_v}{\sqrt{(1+2r_v)(1-r_v)}} \\ &= \frac{k_2 r_v}{\sqrt{(1+2r_v)(1-r_v)}}, \text{ where} \end{aligned} \quad (15)$$

$$k_2 = \sqrt{\frac{3k_1\mathcal{V}}{\mu_0}} = \sqrt{\frac{3V^2}{8\pi^2 f^2 \mu_0 u_{ref}}}\ . \quad (16)$$

This in turn can be substituted into (9) to get

$$\begin{aligned} R_L &= \frac{\rho}{\mathcal{V}\delta}\frac{k_2}{\sqrt{(1+2r_v)(1-r_v)}}\left(w + \frac{2k_2}{3w}\sqrt{\frac{1+2r_v}{1-r_v}}\right) \\ &= k_3\left(\frac{w}{\sqrt{1+r_v-2r_v^2}} + \frac{2k_2}{3w(1-r_v)}\right), \text{ where} \end{aligned} \quad (17)$$

$$k_3 = \frac{\rho k_2}{\mathcal{V}\delta} = \frac{\rho}{\mathcal{V}\delta}\ \frac{V}{\pi f \mu_0}\ \sqrt{\frac{3\mu_0}{8u_{ref}}} = \frac{V\delta}{\mathcal{V}}\ \sqrt{\frac{3\mu_0}{8u_{ref}}}. \quad (18)$$

Because u_{ref} is on the order of $1\ \mathrm{J/cm^3}$ as shown in Fig. 2, k_2 is on the order of $1\ \mathrm{m}^2$ for operation at MHz frequencies and below. Moreover, it can be assumed that w is on the order of $1\ \mathrm{cm}$ for MHz frequencies. Thus, the second term in (17) dominates, resulting in the minimum R_L for $r_v = 0$.

Appendix B
$L(R_L)$ for high-frequency inductor model

This appendix describes the optimization of inductor geometry to obtain the relation between L and R_L of the inductor in LC resonant tanks operating in the high-frequency regime as discussed in Section III-B.

It follows from (10) that

$$wb_{tot} = \sqrt{\frac{L\mathcal{V}}{\mu_0}} = k_4, \quad (19)$$

where w and b_{tot} are inductor dimensions, and $\mathcal{V}$ the total resonator volume. Substituting (19) into (11) gives

$$R_L = \frac{\rho k_4}{\mathcal{V}\delta}\ \left(\frac{k_4}{b_{tot}} + \frac{2b_{tot}}{3}\right). \quad (20)$$

Equating the derivative of R_L with respect to b_{tot} to zero gives

$$-\frac{k_4}{b_{tot}^2} + \frac{2}{3} = 0,$$

$$b_{tot,opt} = \sqrt{\frac{3k_4}{2}}, \quad (21)$$

$$R_{L,opt} = \frac{\rho k_4}{\mathcal{V}\delta}\ 2\sqrt{\frac{2k_4}{3}} = \frac{2\sqrt{2}\rho}{3\mathcal{V}\delta}\left(\frac{L\mathcal{V}}{\mu_0}\right)^{3/4}. \quad (22)$$

Acknowledgment

This material is based upon work supported by the National Science Foundation under Grant Nos. 1507773 and 1610719.

References

[1] D. J. Perreault, J. Hu, J. M. Rivas, Y. Han, O. Leitermann, R. C. N. Pilawa-Podgurski, A. Sagneri, and C. R. Sullivan, "Opportunities and challenges in very high frequency power conversion," in *24th Annual IEEE Applied Power Electronics Conference and Exposition (APEC)*, 2009, pp. 1–14.

[2] C. R. Sullivan, D. Yao, G. Gamache, A. Latham, and J. Qiu, "(Invited) Passiv component technologies for advanced power conversion enabled by wide-band-gap power devices," *ECS Transactions*, vol. 41, no. 8, pp. 315–330, 2011.

[3] N. J. Smith, B. Rangarajan, M. T. Lanagan, and C. G. Pantano, "Alkali-free glass as a high energy density dielectric material," *Materials Letters*, vol. 63, no. 15, pp. 1245–1248, 2009.

[4] Q. Li, K. Han, M. R. Gadinski, G. Zhang, and Q. Wang, "High energy and power density capacitors from solution-processed ternary ferroelectric polymer nanocomposites," *Advanced Materials*, vol. 25, no. 36, pp. 6244–6249, 2014.

[5] W. Li, L. Jiang, X. Zhang, Y. Shen, and C. Nan, "High-energy-density dielectric films based on polyvinylidene fluoride and aromatic polythiourea for capacitors," *Journal of Materials Chemistry A*, vol. 2, no. 38, pp. 15 803–15 807, 2014.

[6] C. R. Sullivan, "Layered foil as an alternative to litz wire: Multiple methods for equal current sharing among layers," in *IEEE 15th Workshop on Control and Modeling for Power Electronics (COMPEL)*, 2014, pp. 1–7.

[7] P. A. Kyaw, A. L. F. Stein, and C. R. Sullivan, "High-Q resonator with integrated capacitance for resonant power conversion," in *Applied Power Electronics Conference (APEC), IEEE 32nd Annual*, 2017.

[8] A. L. F. Stein, P. A. Kyaw, and C. R. Sullivan, "High-Q self-resonant structure for wireless power transfer," in *Thirty-Second Annual IEEE Applied Power Electronics Conference and Exposition (APEC)*, 2017.

[9] P. A. Kyaw and C. R. Sullivan, "Fundamental examination of multiple potential passive component technologies for future power electronics," in *IEEE 16th Workshop on Control and Modeling for Power Electronics (COMPEL)*, 2015.

[10] M. Shoyama, T. Naka, and T. Ninomiya, "Resonant switched capacitor converter with high efficiency," in *IEEE 35th Annual Power Electronics Specialists Conference (PESC)*, vol. 5. IEEE, 2004, pp. 3780–3786.

[11] K. Kesarwani and J. T. Stauth, "A comparative theoretical analysis of distributed ladder converters for sub-module PV energy optimization," in *IEEE 13th Workshop on Control and Modeling for Power Electronics (COMPEL)*, 2012, pp. 1–6.

[12] Digi-Key Electronics. Online catalog for surface mount ceramic capacitors. Accessed on: Mar 06, 2017. [Online]. Available: http://www.digikey.com/products/en/capacitors/ceramic-capacitors/60

[13] C. B. Barth, I. Moon, Y. Lei, S. Qin, and R. C. N. Pilawa-Podgurski, "Experimental evaluation of capacitors for power buffering in single-phase power converters," in *IEEE Energy Conversion Congress and Exposition (ECCE)*, 2015, pp. 6269–6276.

[14] TDK. (2015) SEAT 2013 - SElection Assistant of TDK components. Accessed on: Feb 06, 2017. [Online]. Available: https://product.tdk.com/info/en/technicalsupport/seat/index.html

[15] AVX. (2015) Spicap 3.0. Accessed on: Oct. 03, 2015. [Online]. Available: http://www.avx.com/resources/design-tools/

[16] K. Kesarwani and J. T. Stauth, "Resonant and multi-mode operation of flying capacitor multi-level dc-dc converters," in *Control and Modeling for Power Electronics (COMPEL), IEEE 16th Workshop on*, 2015, pp. 1–8.

[17] S. Pasternak, C. Schaef, and J. Stauth, "Equivalent resistance approach to optimization, analysis and comparison of hybrid/resonant switched-capacitor converters," in *Control and Modeling for Power Electronics (COMPEL), IEEE 17th Workshop on*, 2016, pp. 1–8.